Fluorescent heterogeneities in turbid media: limits for detection, characterization, and comparison with absorption

Xingde Li, Britton Chance, and Arjun G. Yodh

The fundamental limits for detection and characterization of fluorescent (phosphorescent) inhomogeneities embedded in tissuelike highly scattering turbid media are investigated. The absorption and fluorescence contrast introduced by exogenous fluorophores are also compared. Both analyses are based on practical signal-to-noise ratio considerations. For an object with fivefold fluorophore concentration and lifetime contrast with respect to the background tissue, we find the smallest detectable fluorescent object at 3-cm depth in tissuelike turbid media to be ~0.25 cm in radius, whereas the smallest characterizable object size is ~0.75 cm in radius, given a model with 1% amplitude and 0.5° phase noise. We also find that, for fluorescence extinction coefficients $\epsilon \leq 0.5 \times 10^5$ cm^{-1} M^{-1}, the fluorescence measurement mode is superior to the absorption mode for detecting an inhomogeneity. The optimal choice of modulation frequency for the frequency-domain fluorescence measurements is also discussed. © 1998 Optical Society of America

OCIS codes: 170.3650, 170.5270, 260.2570, 290.1990, 290.4210, 290.7050.

1. Introduction

Near-infrared (NIR) diffusive light is expected to be a useful diagnostic and imaging probe for highly scattering media such as biological tissue.[1] One interesting and potentially important biomedical application is to detect and localize heterogeneities such as hematomas and tumors in thick tissue.[2] Most studies thus far have focused on endogenous tissue optical properties such as local variations in optical absorption and scattering for contrast between a tissue abnormality and its surroundings. Fundamental limits for detection and characterization of endogenous absorptive and scattering optical inhomogeneities have been investigated.[3] In 6-cm-thick slabs, for example, it has been shown that the smallest detectable

object size is ~0.30 cm in diameter (given an approximately three-fold absorption or approximately two-fold scattering contrast), whereas the smallest characterizable object size is ~1.0 cm in diameter given a practical signal-to-noise ratio (0.3% amplitude noise and 0.08° phase noise).

Although biological tissues contain several intrinsic fluorophores,[4] none is available in the NIR region, and the high absorption makes these fluorophores disadvantageous for thick-tissue diagnosis. Thus exogenous fluorescent and phosphorescent contrast agents in the NIR region have been considered as means to enhance the sensitivity and specificity for tumor detection, imaging, and treatment in deep tissues.[5–14] The underlying ideas in this case bear substantial similarity to positron emission tomography, fluorescence microscopy, and gadolinium-enhanced magnetic resonance imaging[15] (MRI). The approach relies on the fact that some fluorophores (e.g., hematoporphrin and fluorophore-tagged antibodies) preferentially accumulate within the tumor tissue,[16] have environmentally sensitive lifetimes (e.g., owing to fluorescence quencher concentration variation),[17–19] or both.

Clearly it is desirable to estimate the extent to which fluorescent light can be used for tumor detection and characterization. In this paper we aim to quantify these detection and characterization limits. In addition to emitting at the fluorescence wave-

When this study was performed, all the authors were with the University of Pennsylvania, Philadelphia, Pennsylvania 19104. X. D. Li was with the Department of Physics and Astronomy and the Department of Biochemistry and Biophysics. B. Chance was with the Department of Biochemistry and Biophysics, and A. G. Yodh was with the Department of Physics and Astronomy. X. D. Li is now with the Department of Electrical Engineering and Computer Sciences, Massachusetts Institute of Technology, Cambridge, Massachusetts 02139.

length λ_{em}, fluorophores absorb light at an excitation wavelength λ_{ex}. Therefore all exogenous fluorophores also provide absorption contrast at λ_{ex}. A second aim in this paper is to clarify the circumstances under which absorption or emission detection modes should be used with exogenous contrast agents. The answer will depend on such factors as fluorescence quantum yield and extinction coefficient. Finally, diffusive wave modulation frequency can elevate or suppress the fluorescence contrast, and we discuss the optimal choice of modulation frequency for fluorescence measurements in the frequency domain.

We consider a simple breast-tumor model system consisting of a single spherical object embedded in a highly scattering turbid medium, and we consider the frequency-domain experimental scheme throughout this paper. We use analytical solutions of fluorescent diffuse photon density waves[10] (FDPDW's) to calculate the exact fluorescence amplitude and phase at the sample boundaries. We then obtain simulated experimental data by adding random noise to the exact fluorescence signal (amplitude and phase). First we address the fundamental limits for using FDPDW's to detect and characterize tumors by considering a practical fluorophore concentration–lifetime contrast and a realistic signal-to-noise ratio. We then compare the fluorescence and absorption contrast introduced by exogenous fluorophores. Finally we suggest a simple criterion for choosing a modulation frequency to elevate the fluorescence contrast. The results of this analysis may serve as a guideline for design and selection of exogenous contrast agents.

2. Summary of Analytical Solutions

In a thick highly scattering medium such as biological tissue, NIR light transport is often well approximated as a diffusive process. Microscopically, when the medium's absorption length is much longer than its scattering length (as is the case for NIR light in many biological tissues), each photon experiences multiple scattering events before its absorption or its transmission through the sample boundaries. When a sinusoidal intensity-modulated light source is coupled into the medium (as in all frequency-domain experiments), the diffusive photons add incoherently to produce a scalar photon density wave propagating outward from the source. This scalar wave is referred to as a diffuse photon density wave (DPDW).[1]

Next, suppose that the turbid medium contains a distribution of fluorophores. The fluorophores may be excited by the incident DPDW at optical wavelength λ_{ex}. When the excited fluorophores radiatively relax, fluorescent photons are generated that, again, propagate diffusively through the turbid medium. Collectively a FDPDW is created by addition of the emissions from all fluorophores in the medium. We adopt the following notation in the present discussion: optical properties related to the homogeneous background medium (i.e., outside the object)

Table 1. Chromophore Optical Properties at λ_{ex} and λ_{em} and Source Modulation Frequency[a]

Background				Inhomogeneity			
λ_{ex}		λ_{em}		λ_{ex}		λ_{em}	
μ_{a1}^c	μ_{s1}'	μ_{a1f}^c	μ_{s1f}'	μ_{a2}^c	μ_{s2}'	μ_{a2f}^c	μ_{s2f}'
0.02	8.0	0.025	8.0	0.0205	8.0	0.0256	8.0

[a]The optical properties given in this table are in units of inverse centimeters. The source modulation frequency is 200 MHz unless stated explicitly elsewhere.

are indicated by a subscript 1, e.g., μ_{a1}, μ_{s1}'; optical properties related to the object are indicated by a subscript 2, e.g., μ_{a2}, μ_{s2}'; optical properties related to the fluorescent (or emission) DPDW's are indicated with an extra subscript f. We use a superscript c to indicate chromophore-related parameters (see Table 1).

The analytical solution for the FDPDW in a piecewise homogeneous infinite turbid medium consisting of a spherical object in an otherwise homogeneous background can be written as the superposition of the homogeneous FDPDW Φ_{homo}^{flr} and a scattered FDPDW Φ_{sc}^{flr} (Ref. 10; also see Appendix A); i.e.,

$$\Phi_{hetero}^{flr}(\mathbf{r}_s, \mathbf{r}_d, \omega, a) = \Phi_{homo}^{flr}(\mathbf{r}_s, \mathbf{r}_d, \omega) + \Phi_{sc}^{flr}(\mathbf{r}_s, \mathbf{r}_d, \omega, a)$$

$$= \frac{\epsilon q_1 \eta_1 N_1}{1 - i\omega\tau_1} F_1(\mathbf{r}_s, \mathbf{r}_d, \omega)$$

$$+ \frac{\epsilon q_2 \eta_2 N_2}{1 - i\omega\tau_2} F_2(\mathbf{r}_s, \mathbf{r}_d, \omega, a). \qquad (1)$$

Here $\mathbf{r}_s$ and $\mathbf{r}_d$ are the source and the detector positions, respectively, a is the radius of the inhomogeneity, and ω is the angular source modulation frequency; e.g., $\omega = 2\pi f$, where f is what we generally call the modulation frequency. N_1 and τ_1 are the fluorophore concentration and lifetime, respectively, in the homogeneous background medium (e.g., outside the spherical inhomogeneity); N_2 and τ_2 are the concentration and lifetime inside the inhomogeneity. ϵ is the fluorophore extinction coefficient at the excitation wavelength λ_{ex}. $\eta_1(\eta_2)$ is the fluorescence quantum yield outside (inside) the object. For simplicity, we set $\eta_1 = \eta_2 = 10\%$ in this discussion. q_1 (q_2) is the quenching factor (defined below) for the fluorophores outside (inside) the object. The analytical solution [Eq. (1)] has been verified with finite-difference numerical calculations.[10]

Suppose that the natural radiative decay rate of the fluorophore is Γ_0. In the presence of quenchers, fluorophores in excited states can also decay to their ground states through nonradiative channels. Therefore the total decay rate Γ increases; e.g., $\Gamma = \Gamma_0 + K_D[Q]$. Here $[Q]$ is the quencher concentration and K_D is the Stern–Volmer quenching constant.[20] The quenching factor q is the ratio of the radiative decay rate Γ_0 to the total decay rate Γ; e.g., $q = \Gamma_0/\Gamma = \tau/\tau_0$, where τ_0 and τ are, respectively, the radiative lifetime and the total lifetime of the fluorophore in the presence of the quencher. In biology, paramag-

netic oxygen ($^3O_2$) is a common quencher for almost all fluorophores. The oxygen concentration $[Q_2]$ in the tumor can be two to four times lower that in the surrounding normal tissues $[Q_1]$ because of the high oxygen consumption rate within the tumor.[21] In this case fluorophores within the tumor are quenched less than the fluorophores in the surrounding normal tissues, and the lifetime within the tumor, τ_2, is longer than that of the surrounding normal tissues, τ_1. The quenching factors outside and inside the tumor are $q_1 = \tau_1/\tau_0$ and $q_2 = \tau_2/\tau_0$. We find that the quenching factor is proportional to the lifetime, and it is higher within the tumor than that in the normal tissue ($q_2 > q_1$) if the oxygen concentration is lower in the tumor. It has been suggested that this quenching effect $q_{1,2}$ combined with the demodulation factor $1/(1 - \omega\tau_{1,2})$ provides us the physiological and biochemical basis for using fluorophore lifetime contrast for tumor detection.[14,17,19]

The first term on the right-hand side of Eq. (1) is the analytical solution of the FDPDW in a homogeneous fluorescent turbid medium; e.g., $\Phi^{\text{flr}}_{\text{homo}} = (\epsilon q_1 \eta_1 N_1)/(1 - i\omega\tau_1) F_1$, where the function F_1 has a simple form (for details see Appendix A). It depends on the optical properties of homogeneous background medium at both excitation and emission wavelengths. In the presence of exogenous fluorophores the total background absorption coefficient is the sum of the endogenous chromophore absorption and the exogenous fluorophore absorption; e.g., the total absorption at λ_{ex} of the homogeneous fluorophore-containing background medium is $\mu_{a1} = \mu^c_{a1} + \epsilon N_1$, where μ^c_{a1} is the endogenous absorption that is due to the tissue chromophores and N_1 is the concentration of exogenous background fluorophore. Most fluorophores have rather broad absorption spectra. In addition, we also account for the self-absorption effect of fluorophores by approximating the fluorophore extinction coefficient at fluorescence wavelength λ_{em} as one tenth of that at λ_{ex}, e.g., $\epsilon_f = 0.1\epsilon$. The total absorption at λ_{em} is then $\mu_{a1f} = \mu^c_{a1f} + \epsilon_f N_1$. We can easily obtain the absorption for the medium inside the object by replacing N_1 with the fluorophore concentration inside the object, N_2. The change of the scattering coefficients can also be incorporated into Eq. (1). In general the molecular size of the fluorophore is small. So the change of scattering introduced by the fluorophore is small. Therefore we simply neglect the change of the scattering coefficient that is due to the presence of the exogenous fluorophores.

The second term on the right-hand side of Eq. (1) denotes the scattered wave, e.g., $\Phi^{\text{flr}}_{\text{sc}} = (\epsilon q_2 \eta_2 N_2)/(1 - i\omega\tau_2)F_2$. F_2 has a rather complicated functional dependence on many parameters, such as the optical properties at λ_{ex} and λ_{em}, the fluorophore concentration inside–outside the object, the size and the position of the object, the source–detector positions, and the source modulation frequency (see Appendix A and Ref. 10). It can be written as the sum of multipole moments of all orders (spherical Bessel functions and spherical Hankel functions of the first kind), e.g.,
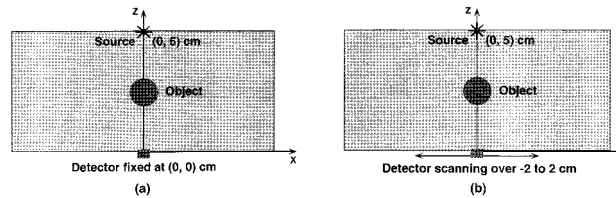

Fig. 1. Infinite slab with one side at $z = 0$ cm and the other side at $z = 5$ cm. (a) Single source–detector geometry. The source and the detector are fixed as shown. A single object is centered between the source and the detector at (0, 2.5) cm. The FDPDW is calculated under this single source–detector configuration for the detection limits analysis. (b) Source position fixed as shown. The detector scans along one side of the slab (x axis) in steps of 0.2 cm. The fluorescence amplitudes and phases at 21 detector positions are calculated for characterization limits analysis.

$\Phi^{\text{flr}}_{\text{sc}}$ = monopole + diopole + quadrapole + higher order. The dominant term is the monopole moment. Different moments have different functional dependences on the radius of the object (a) and on the fluorophore concentration inside the object (N_2). If we Taylor expand different moments with respect to the radius a and the concentration N_2, we find that the monopole moment is related to the concentration and radius through $N_2 a^3$, which is the total number of fluorophores inside the object; the dipole moment is related to $N_2 a^5$. Inasmuch as object size a and fluorophore concentration N_2 appear in the scattered wave as a product, it is essential that at least two multipole moments (e.g., the monopole and the dipole moments) exceed the noise level to characterize a and N_2 simultaneously. We discuss this point in detail in Subsection 5.C. On the other hand, the lifetime dependence of the moments is simple. Different moments have the same functional dependence of the moments is simple. Different moments have the same functional dependence on the lifetime through $q_2/(1 - i\omega\tau_2) \sim \tau_2/(1 - i\omega\tau_2)$. This fact can be seen from Eq. (1), in which the lifetime is an overall factor associated with the scattered wave. Thus we see that the simultaneous characterization of lifetime τ_2 and concentration N_2 is relatively easier than the simultaneous characterization of concentration N_2 and radius a.

3. Models and Criteria

The model that we consider in this paper is an infinitely long slab with a finite width of 5 cm (Fig. 1). An excitation light source modulated at 200 MHz is placed upon the surface of one side of the slab, and a detector is placed upon the opposite side. A single spherical inhomogeneity is embedded at the center of the slab, and it is aligned with the source. Extrapolated zero boundary conditions are applied, leading to an infinite (but convergent) series of image source–object pairs[22–24] (Fig. 2). We then can use the analytical solution for an infinite medium to calculate the forward FDPDW's that correspond to the real source–object pair and each image source–object pair, and superpose those FDPDW's to obtain the total
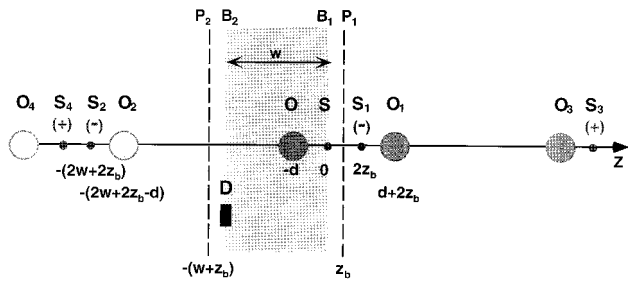
Fig. 2. Extrapolated zero boundary conditions are incorporated into the forward FDPDW calculations by introduction of a series of image source–object pairs. Planes B_1 and B_2 are the two physical surfaces of the slab turbid medium. Planes P_1 and P_2 are the extrapolated boundaries a distance $z_b = 0.704/\mu'_s$ from the corresponding physical surfaces B_1 and B_2. The fluorescence photon fluence is approximated to be zero on the extrapolated boundaries P_1 and P_2. The thickness of the slab is denoted w. The source (S) is at $z = 0$, the object (O) is at $z = -d$, and the detector (D) can be anywhere on the physical surfaces or within the slab. S_1–O_1 is the image source–object pair of the real source–object pair S–O with respect to plane P_1; S_1–O_1 and S–O are mirror symmetric about plane P_1. S_2–O_2 is the image source–object pair of the real source–object pair S–O with respect to plane P_2; S_2–O_2 and S–O are symmetric about plane P_2. S_3–O_3 is the image source–object pair of the image source–object pair S_2–O_2 with respect to plane P_1; S_3–O_3 and S_2–O_2 are symmetric about plane P_1. Series of image source–object pairs can go on following a simple observation. The signs of the image sources are also indicated here. The total FDPDW is the superposition of the FDPDW's generated by the real source–object pair S–O and all the image source–object pairs S_i–O_i with appropriate signs for the image sources. The series converges fast because the fluorescence photon fluence decays exponentially with respect to the (image) source–detector separation.

FDPDW for the slab geometry. For the detection limit study, we calculate the fluorescence wave for a single detector geometry in which the detector is aligned with the source such that the object is centered between the source and the detector [Fig. 1(a)]. For the characterization study, we keep the source position fixed and scan the detector along one side of the slab (x axis) over a 4-cm (-2, 2) region with 0.2-cm step size [Fig. 1(b)]. The fluorescence diffusive wave (amplitude and phase) is then calculated for 21 different detector positions. Throughout the discussion, the endogenous chromophore optical properties of the object and the surrounding background medium are kept fixed while we vary the fluorophore concentration and lifetime as well as the object size.

The criteria that we use to determine the detection and characterization limits are based on a signal-to-noise ratio analysis. We assume a perfect optical filter to reject the background excitation light completely. We come back to discuss the practical requirements for the optical filter in Section 6. In general our system is not limited by shot noise. Consider a 3-mW excitation light source. This corresponds to an excitation photon fluence of $\sim 10^{16}$ photons/s. Given typical fluorophore concentration, lifetime, and optical properties (see Tables 1 and 2), the detected fluorescence fluence is $\sim 10^{10}$ photons/s

Table 2. Quantum Yield η, Background Fluorophore Concentration N_1, Lifetime τ_1, and Extinction Coefficients ϵ and ϵ_f[a]

η	N_1	τ_1	ϵ (at λ_{ex})	ϵ_f (at λ_{ex})
10%	0.1 μM	1.0 ns	0.5×10^5 cm^{-1} M^{-1}	0.05×10^5 cm^{-1} M^{-1}

[a]The quantum yield is fixed at 10% for background fluorophores and fluorophores inside the object. The fluorophore extinction coefficient at the fluorescence wavelength λ_{em} is one tenth of that at the excitation wavelength λ_{ex}, e.g., $\epsilon_f = 0.1\epsilon$. Throughout the paper the extinction coefficients are fixed to these values unless stated otherwise.

for a 5-cm source–detector separation and an active detection area of 0.3-cm diameter. Even when we take into account a loss by another factor of 10^3 that is due to the optoelectrical conversion quantum efficiency of the detector and to other optical couplings, we still have a fluorescence fluence of $\sim 10^7$ photons/s, which corresponds to a shot noise of $\sim 3 \times 10^{-4}$ in 1 s. In practice, other noise from electronics or positional uncertainties will exceed this shot noise. For simplicity, we then consider 1% (10^{-2}) amplitude and 0.5° phase random noise in our noise model.

For studies of detection limits we consider the relative amplitude and phase of the FDPDW, e.g., $|\Phi^{flr}_{hetero}/\Phi^{flr}_{homo}| - 1$ and $[\text{Arg}(\Phi^{flr}_{hetero}) - \text{Arg}(\Phi^{flr}_{homo})]$, respectively. They represent the fractional amplitude and the relative phase perturbation to the FDPDW caused by the inhomogeneity. When either the fractional amplitude or the relative phase perturbation is greater than the system noise level, e.g., $|\Phi^{flr}_{hetero}/\Phi^{flr}_{homo}| - 1 > 1\%$ (or $|\Phi^{flr}_{hetero}/\Phi^{flr}_{homo}| < -1\%$) in amplitude or $|\text{Arg}(\Phi^{flr}_{hetero}) - \text{Arg}(\Phi^{flr}_{homo})| > 0.5°$ in phase, we say that the inhomogeneity is detectable.

For studies of characterization limits we first calculate the amplitude and the phase of the fluorescence diffusive wave, using the analytical solutions.[10] We simulate the experimental data by adding 1% noise randomly to the amplitude and 0.5° noise randomly to the phase. We then employ a χ^2 fitting procedure to determine the fluorophore concentration or lifetime or the size of the inhomogeneity, while assuming that all other parameters are known (e.g., are determined by other imaging modalities such as x-ray, ultrasound, or MRI independently or in conjunction with the optical method). Clearly the situation that we consider here is a best-case one. When the fitted parameters have less than 20% fractional uncertainties relative to their true values, we say that the inhomogeneity is characterizable.

4. Detection Limits

Consider a turbid medium of the slab geometry shown in Fig. 1(a). The amplitude and the phase of the FDPDW will depend on the concentration and lifetime as well as on other parameters. We consider fluorescent dyes, e.g., ICG, which is approved by the U.S. Food and Drug Administration for diagnostic purposes, that have lifetimes of roughly 1 ns and concentrations of roughly 0.1 μM.[25] We first consider a fixed background-fluorophore concentration
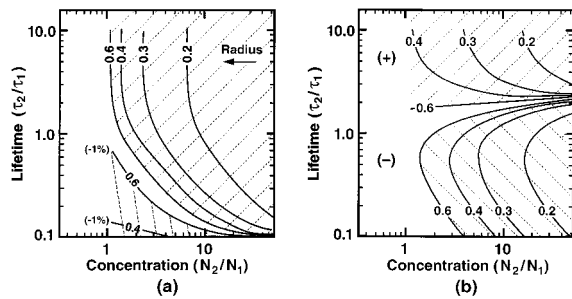
Fig. 3. Contour plots of fractional amplitude and relative phase change versus fluorophore concentration (N_2/N_1) and lifetime variation (τ_2/τ_1) for different-sized objects. The radii are indicated in units inverse centimeters. (a) Curves, 1% fraction amplitude perturbation contours. Hatched areas, fractional amplitude change greater than 1% (or less −1%). (b) Curves, 0.5° relative phase change contours. Hatched areas, relative phase change greater than 0.5° (or less than −0.5°).

$N_1 = 0.1$ μM and a lifetime $\tau_1 = 1.0$ ns (Table 2). Thereafter the perturbation to the FDPDW introduced by the inhomogeneity will depend only on the relative values of fluorophore concentration contrast N_2/N_1 and lifetime contrast τ_2/τ_1. Later we discuss how the absolute background-fluorophore concentration and lifetime affect the relative amplitude and phase of FDPDW, $|\Phi_{\text{hetero}}^{\text{flr}}/\Phi_{\text{homo}}^{\text{flr}}| - 1$ and $[\text{Arg}(\Phi_{\text{hetero}}^{\text{flr}}) - \text{Arg}(\Phi_{\text{homo}}^{\text{flr}})]$, for a fixed fluorophore concentration contrast N_2/N_1 and lifetime contrast τ_2/τ_1. The administration of exogenous fluorescent contrast agents is more desirable when the optical inhomogeneity is intrinsically weak. In this paper we assume that the difference of endogenous optical properties between the inhomogeneity and the surrounding background tissue is small (Table 1). Thus the detection contrast is mainly from the exogenous contrast agents.

A.   Relative Concentration and Lifetime Variation Contrast

For different sizes of spherical inhomogeneities the amplitude and the phase of the FDPDW are calculated over a broad range of fluorophore concentration and lifetime contrast. The fractional amplitude perturbation and relative phase change contours are plotted in Fig. 3. The curves represent the 1% fractional amplitude contours and 0.5° relative phase contours for different object sizes. The hatched areas indicate the fractional amplitude (relative phase shift) greater than 1% (0.5°). Before making a detailed analysis, we find qualitatively that higher fluorophore concentration contrast (N_2/N_1) and higher lifetime contrast (τ_2/τ_1) result in greater amplitude and phase perturbations and therefore permit detection of smaller objects.

   Now let us study why the contours follow the trends indicated by Fig. 3. First consider the dependence of the FDPDW amplitude on the fluorophore concentration inside the object, N_2. The fluorophore concentration has two opposing effects on the amplitude of the FDPDW. On the one hand, given a higher fluorophore concentration, more fluorophores

per unit volume will be excited and therefore more fluorescent photons will be produced; on the other hand, higher fluorophore concentration increases the total absorption coefficients for both the excitation and the emission light. This result will then reduce the excitation and emission photon fluence. The latter effect will not be important when the absolute concentration of the contrast agent is low. From the practical and clinical point of view, the fluorophore concentration has to be low enough (e.g., <1 μM) to avoid serious phototoxicity. For fluorophore extinction coefficients ε near 0.5×10^5 cm^{-1} M^{-1} the additional absorption introduced by the exogenous fluorophore at ~1-μM concentration is roughly in the range of the endogenous tissue chromophore absorption, e.g., $N_2\epsilon \sim 0.05$ cm^{-1}. Under this condition, the perturbation to homogeneous fluorescent photon fluence by the object will be roughly proportional to the fluorophore concentration. As shown in Fig. 3(a), for a given fluorophore lifetime τ_2, as the fluorophore concentration N_2 increases, the object size required to produce the same amount of amplitude (1%) and phase (0.5°) perturbation decreases, and therefore a smaller object can be detected.

   The dependence of fluorescence amplitude on the fluorophore lifetime inside the object is apparent. Equation (1) indicates that the fluence is proportional to $|\tau_2/(1 - i\omega\tau_2)| = \tau_2/(1 + \omega^2\tau_2^2)^{1/2}$, where ω is the angular intensity modulation frequency of the source and τ_2 is the fluorophore lifetime in the object (e.g., tumor). Consider the change of lifetime τ_2 that is due to quenching (q_2). An increase in lifetime (τ_2) introduces two competing effects on the fluorescence fluence. On the one hand, longer lifetimes indicate less quenching for the fluorophores because $q_2 \propto \tau_2$; therefore the fluorescence fluence will increase. On the other hand, longer lifetimes cause a greater demodulation [$\propto 1/(1 - i\omega\tau_2)$]; therefore the fluorescence fluence will decrease. Combining these two effects, we find that overall the fluorescence fluence will first increase as the lifetime τ_2 increases at a fixed fluorophore concentration N_2. When the lifetime reaches a value that is greater than the source modulation period, e.g., $\tau_2 > 2\pi/\omega$, these two effects cancel and the fluorescence fluence then reaches its saturation state [Fig. 3(a)].

   The dependence of relative phase shift on fluorophore concentration N_2 is less obvious. Loosely speaking, the phase is related to the average photon path length of the detected photons. A longer path length corresponds to a larger phase shift. Higher fluorophore concentration increases the absorption coefficient. Consequently, the survival probability of photons with longer path length decreases. The resultant average path length is then reduced. Therefore the relative phase shift decreases as the fluorophore concentration increases. The relative phase shift is related to the lifetime in the tumor by $\tan^{-1}(\omega\tau_2)$ [see Eq. (1)]. A longer lifetime corresponds to a greater phase shift. This effect on the relative phase shift is opposite that which results from the increase of the fluorophore concentration.

Therefore in the lower-left corner of the phase contour plot in Fig. 3(b), where the phase shift is dominated by the concentration contrast, we observe negative relative phase changes, whereas in the upper-right corner, where the phase shift is dominated by the lifetime contrast, we observe positive relative phase changes.

The detection limits depend on the fluorophore contrast (N_2/N_1 and τ_2/τ_1) as well as on the detection system's noise level. Suppose that in practice we have fivefold fluorophore concentration and lifetime variation ($N_2/N_1 = 5$ and $\tau_2/\tau_1 = 5$). If our detection system is limited by 1% noise in amplitude and 0.5° in phase, we find from Fig. 3 that the smallest detectable object size is ~0.25 cm in radius. Given a higher fluorophore concentration contrast (e.g., $N_2/N_1 = 10$), a larger lifetime variation (e.g., $\tau_2/\tau_1 = 10$), and a lower detection system noise level, a smaller object (e.g., 0.15 cm in radius) can then be detected.

B. Effect of Absolute Concentration and Lifetime Variation

The perturbation of the FDPDW also depends on the absolute background-fluorophore concentration N_1 and lifetime τ_1. The total background absorption increases as the background-fluorophore concentration increases. If we keep the concentration contrast N_2/N_1 fixed, the perturbation decreases slightly (in a nonlinear fashion) as the background concentration N_1 increases. This is so simply because less excitation light will reach the object from the source and less fluorescent light will reach the detector from the fluorescent object.

Following the same analysis as that in the early part of this section and assuming that we have the same contrast ($N_2/N_1 = 5$ and $\tau_2/\tau_1 = 5.0$) and the same detection sensitivity (1% in amplitude and 0.5° in phase), when the background-fluorophore concentration increases from 0.1 to 0.5 μM we find that the smallest detectable object is ~0.30 cm in radius (compared with 0.25 cm in radius for lower background concentration $N_1 = 0.1$ μM). On the other hand, the perturbation of FDPDW has a simpler dependence on fluorophore lifetimes (τ_1 and τ_2), e.g., the amplitude perturbation $\sim(\tau_2/\tau_1)[(1 + \omega^2\tau_1^2)/(1 + \omega^2\tau_2^2)]^{1/2}$ and phase perturbation $\sim[\tan^{-1}(\omega\tau_2) - \tan^{-1}(\omega\tau_1)] = \{\tan^{-1}[(\tau_2/\tau_1)\omega\tau_1] - \tan^{-1}(\omega\tau_1)\}$. If we keep the relative lifetime contrast (τ_2/τ_1) fixed, both the amplitude and the phase perturbation decrease as the background-fluorophore lifetime τ_1 increases. For example, given the same relative concentration and lifetime (e.g., $N_2/N_1 = 5$ and $\tau_2/\tau_1 = 5$), when the absolute background-fluorophore lifetime increases from 1.0 to 5.0 ns we find that the smallest detectable object size is ~0.32 cm in radius (compared with 0.25 cm in radius for a shorter background lifetime $\tau_1 = 1.0$ ns).

5. Characterization Limits

Detection of an object does not imply that we can characterize the object. Characterization is more dif-

ficult. Complete characterization includes determination of all parameters of a heterogeneous medium. For a simple case in which there is one spherical object embedded in an otherwise homogeneous-background turbid medium, these parameters are the endogenous absorption and scattering coefficients of the object and the background at the excitation and the emission wavelengths (eight parameters), the fluorophore concentration and lifetime inside and outside the inhomogeneity (four parameters), and the size and the position of the inhomogeneity (four parameters). So we have a 16-parameter set. To explore the limits to which the FDPDW can be fully used to characterize a fluorescent object, we simplify the problem by assuming that only a few parameters are unknown and all others are known (e.g., determined by other modalities such as ultrasound or MRI independently, or in conjunction with the optical method). There are two situations that we consider. First, we simultaneously characterize the fluorophore concentration (N_2) and lifetime (τ_2) inside the inhomogeneity with an assumption that all other parameters are known. Second, we simultaneously characterize the interior fluorophore concentration (N_2) and the size of the inhomogeneity (a), assuming again that all the other parameters are known. The two situations that we consider here are therefore best-case ones.

A. Characterization of an Object with a Known Size

For this case we calculate the FDPDW by using the exact analytical solutions for which the object size is kept at 0.5 cm in radius. The source position is fixed, and the detector scans over $(-2.0, 2.0)$ cm along the x axis with steps of 0.2 cm [Fig. 1(b)]. We then have 21 amplitude and 21 phase exact data points in total. The experimental data (measurements) are simulated by addition of 1% amplitude and 0.5° phase random noise to the exact data. We then apply the χ^2 fitting procedure to characterize simultaneously the fluorophore concentration and lifetime of the fluorescent object, assuming that all other parameters are known. The χ^2 to be minimized is the weighted difference between the measurements and the theoretical estimate, i.e.,

$$\chi^2(N_2, \tau_2) = \sum_{i=1}^{21} \left\{ \frac{[A_{i,M}(N_2, \tau_2) - A_{i,Th}(N_2, \tau_2)]^2}{\delta_A^2} + \frac{[\theta_{i,M}(N_2, \tau_2) - \theta_{i,Th}(N_2, \tau_2)]^2}{\delta_\theta^2} \right\}, \quad (2)$$

where $A_{i,M}$ and $\theta_{i,M}$ are the amplitude and the phase of the ith measurements, respectively (one of 21 measurements along the x axis), and $A_{i,Th}$ and $\theta_{i,Th}$ are the amplitude and the phase of the corresponding theoretical predictions. δ_A and δ_θ are the amplitude and phase errors in corresponding measurements. The minimization is done by use of the Simplex Down-hill subroutine in *Numerical Recipes in C*.[26] For any given fluorophore concentration and lifetime, we take five scans by using different seeds for the random-noise generator. We then fit these five data
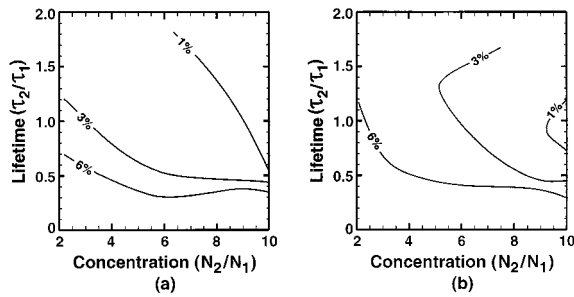
Fig. 4. Characterization limits for an object of a known size (radius $a = 0.5$ cm). (a) characterization uncertainties in fluorophore concentration N_2. For a given lifetime the uncertainty is smaller for a higher concentration; for a given fluorophore concentration the uncertainty is smaller for a longer lifetime. (b) Characterization uncertainties in lifetime τ_2. For a given lifetime the uncertainty is smaller for a higher concentration; for a given concentration the uncertainty is smaller for a greater lifetime variation. See Subsection 5.A for explanations.

Fig. 5. Example of χ^2 distribution versus fitting parameters in characterization of an object with a known size. Fluorophore concentration N_2 and lifetime τ_2 are the two fitting parameters, which we characterize simultaneously. (a) χ^2 versus concentration for a long and a short lifetime (τ_2). A longer lifetime ($\tau_2/\tau_1 = 1.7$) corresponds to a narrower valley. (b) χ^2 versus lifetime for a high and a low concentration (N_2). A higher concentration ($N_2/N_1 = 6$) corresponds to a narrower valley.

sets separately. The fitting results can be different for these five data sets. The standard errors (δN_2 and $\delta \tau_2$) of the fitted parameters are calculated for five scans, and the fractional uncertainties in the concentration and lifetime characterization ($\delta N_2/N_2$ and $\delta \tau_2/\tau_2$) can then be obtained. We repeat the procedure for different fluorophore concentration and lifetime contrast (N_2/N_1 and τ_2/τ_1). The contours of the fractional uncertainties in the fluorophore concentration and lifetime characterization are illustrated in Fig. 4 for a broad range of fluorophore concentration contrast (x axis) and lifetime variation (y axis).

In Section 4 we saw that higher concentrations (N_2) and longer lifetime (τ_2) introduce greater perturbation to the FDPDW, and therefore smaller characterization errors are expected as these parameters are increased. This result is in agreement with the overall trends in Fig. 4. It shows that the characterization error is smaller for higher concentration and longer lifetime. We also notice that the fractional characterization error in lifetime is greater when the lifetime gets longer, which appears surprising in light of the fact that longer lifetimes give rise to greater perturbations. However, note that we consider a 0.5° absolute random phase noise and that the absolute phase error propagates into the lifetime through the phase [$\tan^{-1}(\omega\tau_2)$]. Because of the saturation characteristics of the $\tan^{-1}(x)$ function this 0.5° random phase noise will correspond a larger lifetime uncertainty for a larger $\omega\tau_2$. As shown in Fig. 4, if the object size is known by some other means, the fluorescent object can the be characterized very accurately over a broad range of fluorophore concentration contrast ($2 < N_2/N_1 < 10$) and lifetime variation ($0.2 < \tau_2/\tau_1 < 1.8$), e.g., within 6% fractional uncertainties. For an object of a smaller size (e.g., 0.3 cm in radius) and over the same range of concentration contrast and lifetime variation, the characterization uncertainties will be much larger, e.g., $<20\%$, whereas for an object of a greater size (e.g., 0.8 cm in
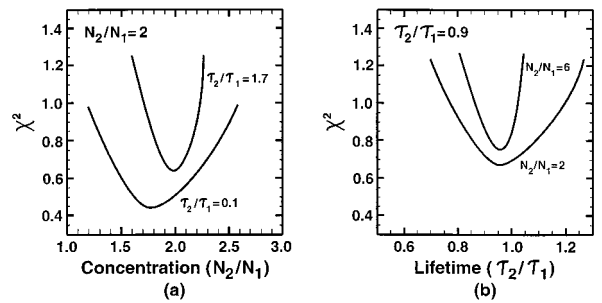
radius) the characterization uncertainties will be much less, e.g., $<3\%$.

Local χ^2 minima are problematic for any fitting procedure. One way to evaluate the fitting quality is to check the χ^2 distribution versus fitting parameters. A good fit will correspond to a minimum χ^2 with a narrow valley. Figure 5(a) illustrates an example of χ^2 versus fluorophore concentration N_2 for two different fluorophore lifetimes ($\tau_2/\tau_1 = 0.1$ and $\tau_2/\tau_1 = 1.7$). We chose these two lifetimes as representatives of a short and a long lifetime. A clear single valley exists for both short and long lifetimes. As we expect, a longer lifetime corresponds to a narrower valley. For comparison, χ^2 versus the fluorophore lifetime τ_2 for two different concentrations ($N_2/N_1 = 2$ and $N_2/N_1 = 6$) is shown in Fig. 5(b). In this case the χ^2 curve has a narrower valley for higher concentration. For other concentrations or lifetimes the χ^2 curves follow the general trends, as illustrated in Fig. 5.

B. Characterization of an Object with an Unknown Size

We next consider the characterization limits for an object with unknown size. For this case we apply the χ^2 minimization procedure and fit for size and concentration simultaneously with all other parameters known. For simplicity, we assume that there is no lifetime contrast (e.g., $\tau_2 = \tau_1$). We follow a procedure similar to that used in Subsection 5.A. The simulated experimental data again have 1% random noise in amplitude and 0.5° random noise in phase. The only difference is that the fitting parameters are the concentration N_2 and the radius a in this case; we minimize χ^2 by varying these two parameters. The contours of the fractional uncertainties in the fluorophore concentration and object radius are presented in Fig. 6 over a broad range of fluorophore concentration (x axis) and object size (y axis). For a given size, the higher the concentration, the smaller the characterization uncertainties; for a given fluorophore concentration, the bigger the object size, the smaller the characterization uncertainties.
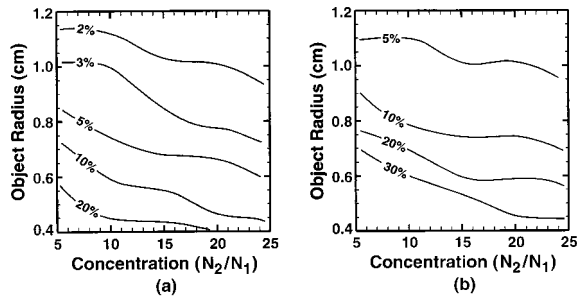
Fig. 6. Characterization limits for an object of an unknown size. (a) Characterization uncertainties in fluorophore concentration N_2. (b) Characterization uncertainties in radius a. In both (a) and (b), for a given object size the uncertainties are smaller for a higher concentration; for a given fluorophore concentration the uncertainties are smaller for a bigger size. The smallest characterizable object size is ~0.75 cm in radius, considering a fivefold concentration contrast and a 20% characterization uncertainty.

Qualitatively speaking, it is easier to characterize a bigger object with higher concentration contrast.

From these contour plots (Fig. 6) we see that, when the object exceeds 0.75 cm in radius, the characterization uncertainties are 20% or less for a fivefold concentration contrast or higher. If we consider a fivefold concentration contrast as a practical obtainable contrast and consider <20% characterization uncertainty as accurate in practice, we find that the smallest characterizable object size is ~0.75 cm in radius. For a higher concentration contrast (e.g., $N_2/N_1 = 20$) we can characterize an object with an even smaller size (e.g., 0.6 cm in radius). The χ^2 curves are also plotted in Fig. 7 to ensure that our fitting results are not trapped in local minima.

C. Multiple Moments Analysis

Given a fivefold concentration contrast, although the smallest detectable object size is ~0.25 cm in radius, the object is not characterizable unless the radius exceeds 0.75 cm because of the functional dependence of the scattered FDPDW on the object size and the concentration. As we discussed in Section 2, the scattered FDPDW is the superposition of different multipole moments. The monopole is related to $N_2 a^3$, whereas the dipole is related to $N_2 a^5$ at the limit of low concentration and small object size (e.g.,
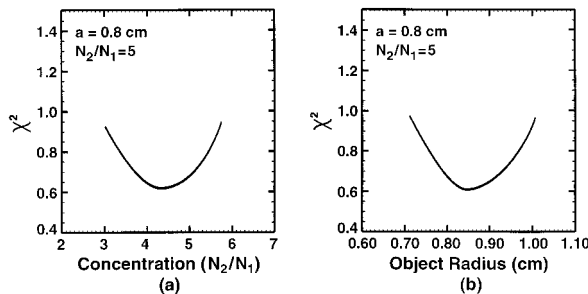

Fig. 7. Example of χ^2 distribution versus fitting parameters in characterization of an object with an unknown size: (a) χ^2 versus concentration and (b) χ^2 versus radius.
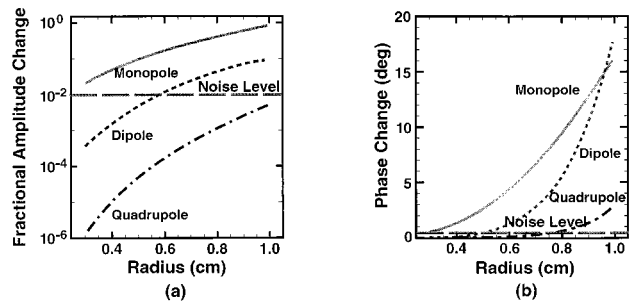

Fig. 8. (a) Fractional amplitude and (b) relative phase changes for different moments versus object size. The concentration contrast is assumed to be fivefold. Horizontal dashed lines indicate 1% amplitude and 0.5° phase noise level. The geometry is given in Fig. 1(a).

when we Taylor expand the moments with respect to N_2 and a). For detection, only the monopole need exceed the noise level; e.g., $|\Phi_{sc}^{flr,l=0}/\Phi_{homo}^{flr}| > 1\%$ or $|Arg(\Phi_{sc}^{flr;l=0}\Phi_{homo}^{flr})| > 0.5°$. On the other hand, whenever two parameters appear as a product in a function, to fit these two parameters simultaneously it is required mathematically that at least two different functional dependencies of the function on these two parameters exist. Therefore for simultaneous characterization of the concentration and size it is necessary for both the monopole and the dipole moments to exceed the noise level. This multipole moments analysis provides us with another way to investigate the detection and characterization limits. Given a fivefold concentration contrast (and no lifetime contrast), we calculate the perturbation of the FDPDW for different multipole moments that are due to objects of different sizes.

The amplitude ($|\Phi_{sc}^{flr,l=0,1,2}/\Phi_{homo}^{flr}|$) and phase [$Arg(\Phi_{sc}^{flr,l=0,1,2}/\Phi_{homo}^{flr})$] perturbation versus object size for the monopole, the dipole, and the quadrapole are plotted in Fig. 8 for different-sized objects, where we also indicate the 1% amplitude and 0.5° phase noise level by horizontal dashed lines. We find that when the object radius exceeds ~0.25 cm the amplitude and the phase of the monopole moment exceed the noise level (1% in amplitude and 0.5°), and this object is thus detectable. Only when the object radius exceeds ~0.6 cm do both the monopole and the dipole moments exceed the noise level, and this object therefore is characterizable. The results of this moment analysis are in agreement with the results from χ^2 fitting and actually provide a more rapid method to assess detection and characterization feasibility.

6. Comparison of Fluorescence and Absorption Contrast

Exogenous fluorophores not only provide fluorescence contrast for tumor detection but also enhance absorption contrast. To compare the fluorescence and absorption contrast induced by exogenous fluorophores we carry out an analysis similar to that in Section 4 for both FDPDW and excitation DPDW; e.g., we are interested only in the amplitude and phase perturbation of the excitation DPDW and FDPDW. Inas-
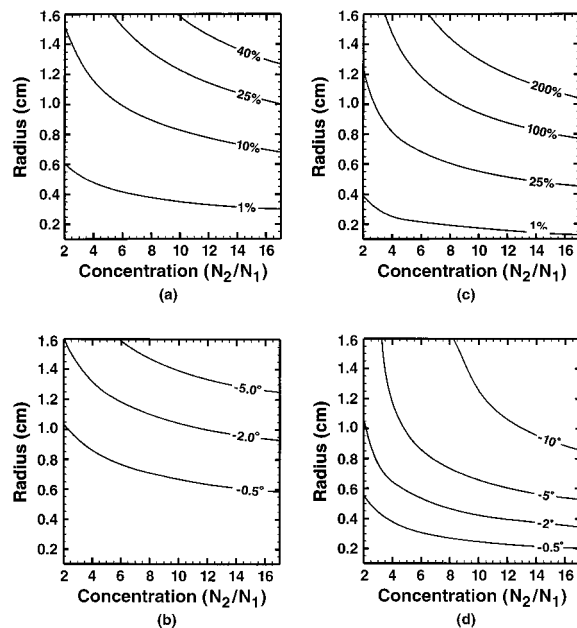
Fig. 9. Contours of fractional amplitude and relative phase changes versus concentration and radius. The lifetime contrast is set to 1 for the fluorescence detection. (a) and (b) show the absorption contrast; (c) and (d) show the fluorescence contrast introduced by exogenous fluorophores.

much as lifetime does not play a role in the absorption measurement, to compare the absorption and fluorescence under the same conditions we simply assume that the lifetimes inside and outside the object are equal ($\tau_2 = \tau_1 = 1$ ns) and therefore that there is no lifetime contrast for the fluorescence detection.

Using the geometry in Fig. 1(a) and analytical solutions for excitation DPDW and FDPDW,[10,27] we calculate the amplitude and phase perturbation for both the excitation DPDW's and the FDPDW's that are due to different-sized objects over a broad range of fluorophore concentration contrast (N_2/N_1); e.g., $\Phi^{ex}_{hetero}/\Phi^{ex}_{homo}$ forthe excitation DPDW and $\Phi^{flr}_{hetero}/\Phi^{flr}_{homo}$ for the FDPDW. The optical properties and other parameters are given in Tables 1 and 2. 1% fractional amplitude and 0.5° phase perturbation contours of the excitation DPDW are shown in Figs. 9(a) and 9(b) for different-sized objects as a function of fluorophore concentration; Figs. 9(c) and 9(d) illustrate the 1% fractional amplitude and 0.5° phase perturbation contours of the FDPDW. Assuming a detection system with 1% amplitude and 0.5° phase noise and utilizing the fluorophore-induced contrast (for both absorption and fluorescence) we see that, for fivefold concentration contrast, the smallest detectable object is ~0.5 cm in radius when we probe the turbid medium using excitation DPDW, whereas the smallest detectable fluorescent object under the same conditions is ~0.25 cm in radius. Comparing Figs. 9(a) and 9(b) with Figs. 9(c) and 9(d), we find that, in general, for a given fluorophore concentration and object size, both the amplitude and the phase perturbation to the FDPDW are greater than those to the

excitation DPDW. Given a perfect optical filter to reject the excitation light in the fluorescence measurement, apparently the detectability is better in the fluorescence mode than in the absorption mode.

In fluorescence measurements, however, given a 3-mW excitation light source that emits ~10^{16} photons/s, the background excitation photon fluence is ~10^{13} photons/s for a 5-cm source–detector separation and an active detection area of 0.3 cm in diameter. Under the same conditions the fluorescent photon fluence is ~10^{10} photons/s (see Tables 1 and 2 for quantum yield, extinction coefficient, and lifetime). Thus the background excitation signal can be 3 orders of magnitude larger than the fluorescence signal. A small amount of excitation light leakage (e.g., 1%) can overwhelm the weak fluorescence signal. Therefore, to measure the fluorescence signal and utilize fully the higher fluorescence contrast introduced by fluorophores for detecting hidden objects, we need an optical filter with a rejection optical density (OD) of >4.0 to suppress the strong background excitation light. As we know [see Eq. (1)], the fluorescence signal is proportional to the fluorophore quantum yield. A filter with a higher rejection OD is correspondingly needed for fluorophores with lower quantum yield. Mathematically the required rejection OD of a filter is scaled by the logarithm of the inverse of fluorophore quantum yield. In the above analysis we assumed a 10% quantum yield. In practice, for fluorophores with much lower quantum yields (e.g., 0.1%) the fluorescence measurement can be difficult. The required rejection OD of the optical filter can be as great as 6.

Different fluorescent contrast agents generally have different extinction coefficients. The relative fluorescence/absorption contrast varies with the extinction coefficient. Consider the geometry in Fig. 1(a) with a spherical object of 0.5-cm radius. Figures 10(a) and 10(b) show the contours of fractional amplitude and phase for the absorption signal at excitation wavelength λ_{em}, and Figs. 10(c) and 10(d) show the contours of fractional amplitude and phase for the fluorescence signal at emission wavelength λ_{ex}. We find that, for a fivefold concentration contrast, the perturbation to the FDPDW can exceed 5% in amplitude and −1° in phase for fluorophores with extinction coefficients lower than ~1.0×10^5 cm^{-1} M^{-1}, whereas the perturbation to the excitation DPDW exceeds 5% in amplitude only when the extinction coefficient is greater than 2.5×10^5 cm^{-1} M^{-1}. Note that the phase perturbation to the excitation DPDW is very small (e.g., <0.5°) over a broad range of the extinction coefficients and concentration contrast. Therefore it is difficult to detect the inhomogeneity by use of fluorescent contrast agents from only the phase measurements of the excitation DPDW. Roughly speaking, if we have an optical filter with an OD of >4 to reject background excitation light, the fluorescence signal provides better contrast for fluorescent contrast agents with lower extinction coefficients; only for higher extinction coefficients
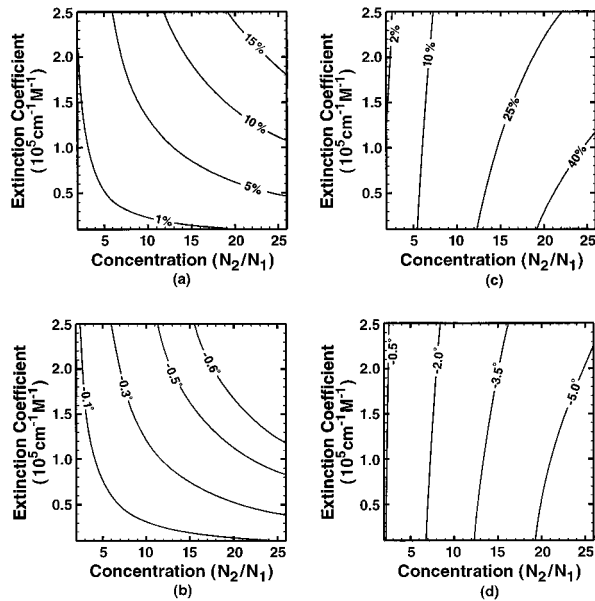
Fig. 10. Contours of fractional amplitude and relative phase changes for (a), (b) absorption and (c), (d) fluorescence contrast versus concentration and extinction coefficient. The object size is 0.5 cm in radius, and the source–detector geometry is shown in Fig. 1(a). For fluorophores with an extinction coefficient near 1.0×10^5 cm^{-1} M^{-1}, we see that the fluorescence contrast is in general greater than the absorption contrast.
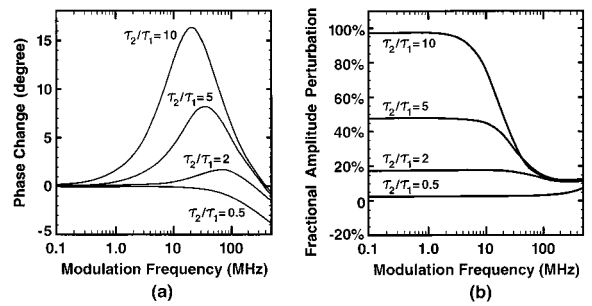

Fig. 11. (a) Fractional amplitude perturbation versus modulation frequency for different lifetime contrasts; (b) relative phase perturbation versus modulation frequency for different lifetime contrasts. Given a lifetime contrast τ_2/τ_1, we find that the amplitude and the phase perturbation that are due to the lifetime contrast will be optimally elevated when the source modulation frequency is appropriately chosen, e.g., $\omega\tau_2 \approx 1$.

(e.g. $\epsilon > \sim 2.5 \times 10^5$ cm^{-1} M^{-1}) is the absorption contrast superior to the fluorescence contrast.

The background-fluorophore concentration is taken to be $N_1 = 0.1$ μM in the above discussion. At a fixed relative concentration contrast N_2/N_1 the background concentration N_1 determines the absolute concentration contrast, and therefore it will also affect the perturbation to both the FDPDW and the excitation DPDW. As we discussed at the end of Section 4, for a fixed relative concentration N_2/N_1 the increase in the background concentration N_1 reduces the detectability of an object probed by the FDPDW. Similar analysis shows that the increase in background concentration N_1, on the other hand, enhances the detectability through the absorption measurement. We have found that, for a given background fluorophore concentration N_1, the fluorescence contrast is better than the absorption contrast at detecting a hidden object when the absorption introduced by the exogenous background fluorophore is low, e.g., $\epsilon N_1 \leq \mu_{a1}^c$, where μ_{a1}^c is the endogenous background absorption.

7. Discussion and Conclusion

It is essential to have multiple data points to characterize an inhomogeneity by use of a χ^2 fitting procedure. So far we have considered multiple measurements by scanning the detector. We chose our scan region from −2 to 2 cm in the above discussion. This scan region was chosen so that source and the detector would be close enough to ensure that the amplitude and the phase perturbations are greater than the system noise level. Measurements made at large source–detector separation will not help to improve the detection or characterization if the perturbation is less the noise level.

An alternative approach to obtaining multiple measurements is to employ multiple modulation frequencies for a single source–detector position.[28] We have found that high modulation frequencies are not desirable. Higher modulation frequencies produce larger wave attenuation factors and therefore lower excitation and fluorescence fluences. As we discussed above (e.g., see Section 4), the lifetime is coupled to the modulation frequency through the demodulation factor $\tau/(1 - i\omega\tau)$. The demodulation introduces an amplitude perturbation $(\tau_2/\tau_1)[(1 + \omega^2\tau_1^2)/(1 + \omega^2\tau_2^2)]^{1/2}$ and a phase shift $[\tan^{-1}(\omega\tau_2) - \tan^{-1}(\omega\tau_1)]$. The amplitude perturbation is roughly proportional to the lifetime contrast τ_2/τ_1 at low modulation frequencies (e.g., $\omega\tau_{1,2} < 1/3$). At high modulation frequencies (e.g., $\omega\tau_{1,2} > 3$), the amplitude perturbation diminishes and becomes independent of the lifetime contrast.

The phase shift follows the trend of the function $\tan^{-1}(x)$. It can be shown that the peak of the phase shift, $\Delta\theta = [\tan^{-1}(\omega\tau_2) - \tan^{-1}(\omega\tau_1)] = \{\tan^{-1}[(\tau_2/\tau_1)\omega\tau_1)] - \tan^{-1}(\omega\tau_1)\}$, which is due to the lifetime contrast τ_2/τ_1, occurs when $\omega\tau_2 = \sqrt{\tau_2/\tau_1}$. Considering all other factors that contribute to the phase shift (such as the concentration contrast and the endogenous absorption contrast), we find that $\omega\tau_2 \approx 1$ gives a simple estimate for the modulation frequency at which we will approximately obtain a maximum phase perturbation.

These features of the amplitude and phase perturbations versus the modulation frequency are shown in Fig. 11 for several lifetime contrasts τ_2/τ_1, where we assume that we have a 0.5-cm-radius object and a fixed concentration contrast ($N_2/N_1 = 5$). Other parameters are given in Tables 1 and 2. Clearly the choice of an appropriate modulation frequency can help in optimal use of the contrast provided by the lifetime contrast, and an inappropriate choice of the

modulation frequency can reduce or demolish the contrast. We can obtain a maximum amplitude perturbation when we employ a dc source ($\omega = 0$), but we will lose the phase information. The rule of thumb for choosing the modulation frequency for fluorescence measurements is that $\omega\tau_2 \sim 1$, which will ensure that we have enough sensitivity to the phase perturbation that is due to the lifetime contrast without degrading the amplitude perturbation too much. This discussion can also apply to phosphorescence with millisecond lifetime ranges for which the optimal modulation frequency would be of the order of kilohertz.

We draw the following conclusions: (1) If our detection system is limited by 1% noise in amplitude and by 0.5° in phase, the smallest detectable fluorescent object size is ~0.25 cm in radius, given a fivefold fluorophore concentration and lifetime contrast. (2) An inhomogeneity can be well characterized within 6% characterization uncertainties if *a priori* information about its size is known. (3) When no *a priori* information about the object size is available, the characterization is then more difficult. The smallest characterizable object size in this case is ~0.75 cm in radius.

For systems with lower noise levels or higher fluorophore concentration contrast, we can then detect and characterize a smaller object. We can also statistically reduce the characterization errors by increasing the number of measurements (e.g., the characterization error $\propto 1/\sqrt{N}$, where N is the total number of measurements).

Finally, in our comparison of the absorption and fluorescence contrast introduced by exogenous fluorophores we find that, given a sufficiently large fluroescence filter OD (e.g., >4) and fluorescence quantum yield (e.g., $\eta > 10\%$), the fluorescence mode of measurements is in general superior to the absorption mode for fluorophores with moderate extinction coefficients. Some fluorophores with higher affinity for tumor tissue have been under investigation.[29,30] These high-contrast fluorophores make the fluorescent probe more promising and attractive for use in tumor detection and imaging.

Appendix A

As was shown in Ref. 10, for a fluorescent spherical object embedded in an infinite fluorescent turbid medium, the FDPDW is the superposition of the FDPDW in a homogeneous fluorescent medium $\Phi^{\text{flr}}_{\text{home}}$ and the scattered FDPDW $\Phi^{\text{flr}}_{\text{sc}}$; i.e.,

$$\Phi^{\text{flr}}_{\text{hetero}}(\mathbf{r}_s, \mathbf{r}_d, \omega, a) = \Phi^{\text{flr}}_{\text{homo}}(\mathbf{r}_s, \mathbf{r}_d, \omega) + \Phi^{\text{flr}}_{\text{sc}}(\mathbf{r}_s, \mathbf{r}_d, \omega, a).$$

$$(A1)$$

Here $\mathbf{r}_s$ and $\mathbf{r}_d$ denote the source and the detector positions, respectively; ω is the source angular mod-

ulation frequency; and a is the object radius. The homogeneous FDPDW $\Phi^{\text{flr}}_{\text{home}}$ is

$$\Phi^{\text{flr}}_{\text{homo}}(\mathbf{r}_d, \mathbf{r}_s, \omega) = A_1 \frac{\epsilon q_1 \eta_1 N_1}{1 - i\omega\tau_1} \left[\frac{\exp(ik_1|\mathbf{r}_d - \mathbf{r}_s|)}{4\pi|\mathbf{r}_d - \mathbf{r}_s|} \right.$$
$$\left. - \frac{\exp(ik_{1f}|\mathbf{r}_d - \mathbf{r}_s|)}{4\pi|\mathbf{r}_d - \mathbf{r}_s|} \right]. \quad (A2)$$

Here A_1 is a constant that depends on the optical properties at both excitation and emission wavelengths (λ_{ex} and λ_{em}) as well as on the excitation source strength; k_1 and k_{1f} are the wave numbers of the diffusive photon density wave that correspond to the optical properties at the excitation and emission wavelengths, respectively; ϵ is the fluorophore extinction coefficient; and N_1, τ_1, η_1, and q_1 are the background fluorophore concentration, lifetime, quantum yield, and quenching factor, respectively.

The scattered FDPDW $\Phi^{\text{flr}}_{\text{sc}}$ can be written as

$$\Phi^{\text{flr}}_{\text{sc}}(\mathbf{r}_d, \mathbf{r}_s, \omega, a) = A_2 \frac{\epsilon q_2 \eta_2 N_2}{1 - i\omega\tau_2}$$
$$\times \left\{ \sum_{lm} [B_{lm} h_l^{(1)}(k_{1f} r) + C_{lm} h_l^{(1)}(k_1 r)] \right.$$
$$\left. \times Y_{lm}(\Omega) \right\}. \quad (A3)$$

Here A_2 is a constant that depends on the optical properties at both excitation and emission wavelengths (λ_{ex} and λ_{em}) as well as on the object size and the excitation source strength; N_2, τ_2, η_2, and q_2 are the fluorophore concentration, lifetime, quantum yield, and quenching factor inside the object, respectively; and B_{lm} and C_{lm} are complicated constants that depend on the optical properties inside and outside the object at the excitation and emission wavelengths (λ_{ex} and λ_{em}), the object size and the excitation source position. $h_l^{(1)}$ is the spherical Hankel function of the first kind, and $Y_{lm}(\Omega)$ is the spherical harmonics. ϵ, k_1 and k_{1f} are the same as in Eq. (A2).

References and Note

1. A. Yodh and B. Chance, "Spectroscopy and imaging with diffusing light," Phys. Today **48**(3), 31–36 (1995), and references therein.

2. See related studies in B. Chance, R. R. Alfano, and A. Katzir, eds., *Optical Tomography and Spectroscopy of Tissue: Theory, Instrumentation, Model, and Human Studies II*, Proc. SPIE **2979** (1997).

3. D. A. Boas, M. A. O'Leary, B. Chance, and A. G. Yodh, "Detec-

tion and characterization of optical inhomogeneities with diffuse photon density waves: a signal-to-noise analysis," Appl. Opt. **36,** 75–92 (1997).

4. R. A. Zangaro, L. Silveira, R. Manoharan, G. Zonios, I. Itzkan, R. R. Dasari, J. VanDam, and M. S. Feld, "Rapid multiexcitation fluorescence spectroscopy system for *in vivo* tissue diagnosis," Appl. Opt. **35,** 5211–5219 (1996).

5. A. Knüttel, J. M. Schmitt, R. Barnes, and J. R. Knutson, "Acousto-optic scanning and interfering photon density waves for precise localization of an absorbing (or fluorescent) body in a turbid medium," Rev. Sci. Instrum. **64,** 638–644 (1993).

6. D. A. Boas, M. A. O'Leary, B. Chance, and A. G. Yodh, "Scattering and wavelength transduction of diffuse photon density waves," Phys. Rev. E **47,** R2999–R3002 (1993).

7. E. M. Sevick-Muraca and C. L. Burch, "Origin of phosphorescence signals reemitted from tissues," Opt. Lett. **19,** 1928–1930 (1994).

8. M. S. Patterson and B. W. Pogue, "Mathematical model for time-resolved and frequency-domain fluorescence spectroscopy in biological tissues," Appl. Opt. **33,** 1963–1974 (1994).

9. M. A. O'Leary, D. A. Boas, B. Chance, and A. G. Yodh, "Reradiation and imaging of diffuse photon density waves using fluorescent inhomogeneities," J. Lumin. **60,** 281–286 (1994).

10. X. D. Li, M. A. O'Leary, D. A. Boas, B. Chance, and A. G. Yodh, "Fluorescent diffuse photon density waves in homogeneous and heterogeneous turbid media: analytic solutions and applications," Appl. Opt. **35,** 3746–3758 (1996).

11. A. E. Cerussi, J. S. Maier, S. Fantini, M. A. Franceschini, W. W. Mantulin, and E. Gratton, "Experimental verification of a theory for the time-resolved fluorescence spectroscopy of thick tissues," Appl. Opt. **36,** 116–124 (1997).

12. E. M. Sevick-Muraca, G. Lopez, J. S. Reynolds, T. L. Troy, and C. L. Hutchinson, "Fluorescence and absorption contrast mechanisms for biomedical optical imaging using frequency-domain techniques," Photochem. Photobiol. **66,** 55–64 (1997).

13. J. Wu, L. Perelman, R. R. Dasari, and M. S. Feld, "Fluorescence tomographic imaging in turbid media using early-arriving photons and Laplace transforms," Proc. Natl. Acad. Sci. USA **94,** 8783–8788 (1997).

14. E. L. Hull, M. G. Nichols, and T. H. Foster, "Localization of luminescent inhomogeneities in turbid media with spatially resolved measurements of cw diffuse luminescence emittance," Appl. Opt. **37,** 2755–2765.

15. P. S. Tofts, B. A. Berkowitz, and M. Schnall, "Quantitative analysis of dynamic Gd-DTPA enhancement in breast tumors using a permeability model," Magn. Res. Med. **33,** 564–568 (1995).

16. B. C. Wilson and M. S. Patterson, "The physics of photodynamic therapy," Phys. Med. Biol. **31,** 327–360 (1986).

17. W. L. Rumsey, J. M. Vanderkooi, and D. F. Wilson, "Imaging of phosphorescence: a novel method for measuring oxygen distribution in perfused tissue," Science **241,** 1649–1651 (1988).

18. J. R. Lakowicz, H. Szmacinski, K. Nowaczyk, and M. L. Johnson, "Fluorescence lifetime imaging of calcium using Quin-2," Cell Calcium **13,** 131–147 (1992).

19. S. A. Vinogradov, L.-W. Lo, W. T. Jenkins, S. M. Evans, C. Koch, and D. F. Wilson, "Noninvasive imaging of the distribution of oxygen in tissue *in vivo* using infrared phosphors," Biophys. J. **70,** 1609–1617 (1996).

20. J. R. Lakowicz, *Principles of Fluorescence Spectroscopy* (Plenum, New York, 1983).

21. P. W. Vaupel, *Blood Flow, Oxygenation, Tissue pH Distribution, and Bioenergetic Status of Tumor* (Ernst Schering Research Foundation, Berlin, 1994).

22. M. S. Patterson, B. Chance, and B. C. Wilson, "Time resolved reflectance and transmittance for the noninvasive measurement of tissue optical properties," Appl. Opt. **28,** 2331–2335 (1989).

23. R. C. Haskell, L. O. Svaasand, T. T. Tsay, T. C. Feng, M. S. McAdams, and B. J. Tromberg, "Boundary conditions for the diffusion equation in radiative transfer," J. Opt. Soc. Am. A **11,** 2727–2741 (1994).

24. R. Aronson, "Boundary conditions for diffusion of light," J. Opt. Soc. Am. A **12,** 2532–2539 (1995).

25. T. R. Carski, "Indocynanine green: history, chemistry, pharmacology, indication, adverse reactions, investigations and prognosis," in *An Investigator's Brochure*, 24 June 1994.

26. W. H. Press, S. A. Teukolsky, W. T. Vetterling, and B. P. Flannery, *Numerical Recipes in C* (Cambridge U. Press, New York, 1992).

27. D. A. Boas, M. A. O'Leary, B. Chance, and A. G. Yodh, "Scattering of diffuse photon density waves by spherical inhomogeneities within turbid media: analytic solutions and applications," Proc. Natl. Acad. Sci. USA **91,** 4887–4891 (1994).

28. J. B. Fishkin, O. Coquoz, E. R. Anderson, M. Brenner, and B. J. Tromberg, "Frequency-domain photon migration measurements of normal and malignant tissue optical properties in a human subject," Appl. Opt. **36,** 10–20 (1997).

29. K. Licha, B. Riefke, and W. Semmler, "Synthesis and characterization of cyanine dyes as contrast agents for near-infrared imaging," in *Optical and Imaging Techniques for Biomonitoring II*, H. Foth, R. Marchesini, and H. Podbielska, eds., Proc. SPIE **2927,** 192–198 (1996).

30. K. W. Woodburn, Q. Fan, D. R. Miles, D. Kessel, Y. Luo, and S. W. Young, "Localization and efficacy analysis of the photo-therapeutic lutetium texaphyrin (PCI-0123) in the murine EMT6 sarcoma model," Photochem. Photobiol. **65,** 410–415 (1997).